PHYSICAL REVIEW D **76,** 054004 (2007)

Larkin-Ovchinnikov-Fulde-Ferrell state in two-color quark matter

Kenji Fukushima[1] and Kei Iida[2]

[1]*RIKEN BNL Research Center, Brookhaven National Laboratory, Upton, New York 11973, USA*
[2]*Department of Natural Science, Kochi University, Akebono-cho, Kochi 780-8520, Japan*

(Received 21 May 2007; published 24 September 2007)

We explore the phase structure of two-color and two-flavor QCD in the space of the quark chemical potential μ_q and the isospin chemical potential μ_I. Using a mean-field model we calculate the chiral and diquark condensates, σ and Δ, self-consistently. In weak coupling and in the chiral limit, we confirm the interval of the isospin chemical potential, $0.71\Delta_0 < \mu_I < 0.75\Delta_0$, in which a single plane-wave Larkin-Ovchinnikov-Fulde-Ferrell (LOFF) phase is favored over isotropic superfluidity and normal quark matter. The LOFF window becomes slightly wider at high density. For stronger coupling with nonzero quark mass, which is relevant to currently available numerical simulations in lattice two-color QCD, the single plane-wave LOFF phase appears only at sufficiently high density. The prediction obtained for the LOFF region could be tested with lattice since we can prove that the present system is free from the fermion sign problem. We draw the energy landscape on which local minima corresponding to the isotropic superfluid phase and the LOFF phase and a local maximum corresponding to the gapless phase are manifest. Our results clearly illustrate the path from the unstable gapless phase down to the LOFF phase.

DOI: 10.1103/PhysRevD.76.054004 PACS numbers: 12.38.Mh, 26.60.+c

I. INTRODUCTION

It is a long-standing problem to uncover the phase structure of dense nuclear and quark matter in the low temperature and high baryon density region because of its complexity. From the academic point of view, our curiosity urges us to imagine what an extreme state of cold quark matter at asymptotic high density is like. In fact, at density far larger than the strange quark mass M_s but still smaller than the charm, bottom, and top quark masses, there has been established a consensus that quark matter takes on color superconductivity in a color-flavor locked (CFL) manner [1,2]. Then, what comes next as the density goes down? This is an important question because, if quark matter appeared in neutron star cores, its state would be strongly affected by M_s. One plausible candidate was considered to be a gapless color superconducting phase [3], which is a QCD version of the Sarma phase [4,5] partially stabilized by neutrality constraints. Specifically the gapless CFL (gCFL) phase [6] was expected in quark matter in the intermediate density region. It turns out, however, that the gapless phase is unlikely to exist in such quark matter because of the chromomagnetic instability that develops at sufficiently low temperatures [7–10]. At higher temperatures, a u-quark superconducting (uSC) phase is predicted to occur as a remnant of the gapless phase [10,11], and the existence of the doubly critical point facing both the uSC phase and a d-quark superconducting phase [12] seems robust [13,14].

Interestingly, the chromomagnetic instability in the gapless phase tends toward spontaneous generation of a total momentum $2\boldsymbol{q}$ carried by each Cooper pair [10,15,16]. [In addition to the chromomagnetic instability, an instability appears with respect to inhomogeneous fluctuations in the gap magnitude, leading the gapless state to a BCS-normal phase separation or a BCS-normal mixed phase [17]. See also Ref. [18].] In general, an inhomogeneous superconducting phase characterized by pairing with nonvanishing $2\boldsymbol{q}$ is referred to as the LOFF phase named after Larkin-Ovchinnikov [19] and Fulde-Ferrell [20]. In the present context, it is possible to describe a state resulting from the same instability in several different ways: a state with current generation of collective excitations [21,22], a state with gluon condensation [23], and a colored LOFF state [10,16]. They are all equivalent algebraically. In terms of the colored LOFF state, the chromomagnetic instability is to be regarded as an instability with respect to the spatially oscillating phase factor, $e^{i\lambda^\alpha \boldsymbol{q}\cdot\boldsymbol{r}}$ with the Gell-Mann matrices λ^α, of the pairing gap matrix in color space. In the present paper which focuses on a two-color theory, we shall generalize the notion of chromomagnetic instability to a *phase instability* that makes sense not only in a charged superconductor but also in a neutral superfluid.

In the LOFF phase the translational and rotational symmetries are spontaneously broken by $\boldsymbol{q}$. The single plane-wave LOFF phase is only the simplest etude and in general a complicated crystal structure should emerge. In the context of QCD physics [24–27], the plane-wave LOFF phase, crystal structure, stability, and its physical property have been examined mainly by means of the high-density effective theory and the Ginzburg-Landau expansion in terms of the pairing gap [28–31]. For the moment it is an urgent problem to clarify the energetically favorable structure of the three-flavor LOFF phase. Whereas the phase instability guarantees existence of the LOFF phase with a lower energy than the gCFL phase even within the single plane-wave ansatz, the high-density effective theory and Ginzburg-Landau approximations do not allow us to identify the most favorable LOFF phase in full details.

We shall here revisit the LOFF phase in two-color and two-flavor QCD in the presence of both the quark chemical potential μ_q and the isospin chemical potential μ_I. It was pointed out in Ref. [32] that the interval of μ_I in which the LOFF phase occurs exists in such a system at least in weak coupling, while it is nontrivial whether the LOFF window should survive or not at stronger coupling with a finite quark mass introduced. We will make use of a mean-field model to address this issue by following a line of argument of Ref. [33], which looks successful in reproducing the numerical results of lattice two-color QCD [34–39].

Although it is beyond our current scope, we expect that the lattice two-color QCD could observe a signature of the LOFF phase numerically. We adopt two sets of the model parameters, one of which is relevant to currently available lattice simulations in which the diquark condensate has been measured at $\mu_q \neq 0$ but $\mu_I = 0$. This work is a first step toward identifying the LOFF state on lattice.

We can also mention that it is instructive to shed light on a two-color QCD as a mimic of real QCD in which the LOFF state is a natural consequence of the phase instability in the gapless state. In the context of real QCD, we know the direction in which the unstable gapless state goes and consider the LOFF state as a natural replacement of the unstable state, but it remains to be surveyed how one gives way to the other. At this point, it is advantageous to switch to two-color QCD. In fact, simplicity inherent in two-color QCD enables us to picture the energy landscape including various states. By doing so, we can get a feeling that we are heading for the right way dictated by real QCD.

This paper is organized as follows. In Sec. II we mention unique features of two-color QCD, our mean-field model, approximations to be made, and the twofold parameter choice at weak and intermediate coupling. Section III is composed of four subsections presenting numerical results from the mean-field model for the isotropic superfluid phase, the unstable gapless phase, the LOFF phase, and the energy landscape, respectively. Our main results are summarized in Fig. 5 for weak coupling with massless quarks and in Fig. 6 for intermediate coupling accessible in the lattice setting. We also plot the free energy in the space of the diquark condensate and the pair momentum in Figs. 7 and 8 for the intermediate coupling case. Section IV is devoted to our conclusions and future perspectives.

II. SETUP

In this section, we will briefly summarize a chiral symmetry breaking pattern inherent in two-color QCD, discuss the absence of the fermion sign problem, and then describe a model for two-color matter with nonzero μ_q and μ_I along with some approximations in calculating the thermodynamic potential. We will emphasize the benefit from the two-color nature that the model prediction is more robust than in the three-color case.

A. Symmetry breaking pattern

Two-color QCD has a peculiar feature of chiral symmetry. When quarks are massless and the chemical potential is zero, chiral symmetry in two-color and two-flavor QCD is augmented from the standard one $\mathrm{SU_L}(2) \times \mathrm{SU_R}(2)$ to SU(4). This is because a doublet and an antidoublet of the SU(2) group are indistinguishable, which makes left-handed quarks and right-handed antiquarks belong to the same group multiplet and hence doubles the basis. In fact this extra symmetry, which is often referred to as the Pauli-Gürsey symmetry [40], amounts to rotational symmetry among the chiral and diquark condensates. The spontaneous chiral symmetry breaking pattern is thus $\mathrm{SU}(4) \to \mathrm{Sp}(4)$ in the presence of diquark condensation. Once a nonzero quark chemical potential sets in, i.e., $\mu_q \neq 0$, the extended symmetry is reduced to standard global symmetry as $\mathrm{SU}(4) \to \mathrm{SU_L}(2) \times \mathrm{SU_R}(2) \times \mathrm{U_B}(1)$. If quarks are massive, the remaining symmetry is as usual $\mathrm{SU_V}(2) \times \mathrm{U_B}(1)$, which spontaneously breaks down to Sp(2) once the quark chemical potential exceeds the mass of the lowest-lying excitations carrying nontrivial baryon number. Because the $\mathrm{U_B}(1)$ symmetry is spontaneously broken by the diquark condensation, the system is a superfluid accompanied by massless Nambu-Goldstone bosons. The gauge symmetry is intact since the diquark condensate is gauge invariant in this case.

It is obvious that no chromomagnetic instability can happen in any kind of superfluid state of this system because no finite Meissner screening mass arises without color symmetry breaking. In other words, if we interpret it as the phase instability as we mentioned above, the color singlet diquark condensate cannot have any spatially oscillating phase in color space and thus cannot lead to any instability involving color degrees of freedom. In terms of the phase instability, on the other hand, we can understand that fluctuations in the $\mathrm{U_B}(1)$ phase in the gapless superfluid state could result in instability. It should be mentioned that the modes in the $\mathrm{U_B}(1)$ phase itself in a superfluid correspond to the massless Nambu-Goldstone bosons, and the instability would not emerge in the phase factor $e^{i2\boldsymbol{q}\cdot\boldsymbol{r}}$ but in the wave-vector $\boldsymbol{q}$ of the phase, i.e., the current of the Nambu-Goldstone boson in a physics language (see Refs. [21,22] for details).

B. Fermion sign problem

In this subsection, we briefly summarize the sign problem of the fermion determinant [41] and make sure that two-color QCD escapes from it for *any* number of quark flavors. The Dirac operator in question reads

$$\mathcal{M}(\mu_q) = \gamma_\mu D^\mu + \gamma_4 \mu_q + m \tag{1}$$

per one quark flavor in Euclidean space, where D^μ denotes the covariant derivative containing gauge fields. In the presence of the isospin chemical potential μ_I with u and d flavors, the Dirac operator is then a direct sum of two

flavor sectors: $\mathcal{M}(\mu_u) \oplus \mathcal{M}(\mu_d)$. For the moment we shall focus on the one-flavor $\mathcal{M}(\mu_q)$ to discuss the sign problem, since $\det\mathcal{M}(\mu_q) \geq 0$ is sufficient to claim $\det[\mathcal{M}(\mu_u) \oplus \mathcal{M}(\mu_d)] = \det\mathcal{M}(\mu_u) \cdot \det\mathcal{M}(\mu_d) \geq 0$.

Because the Euclidean gamma matrices γ_μ's are Hermitian by convention, the eigenvalue λ_n of anti-Hermitian $\gamma_\mu D^\mu$, i.e.,

$$\gamma_\mu D^\mu \psi_n = \lambda_n \psi_n, \tag{2}$$

is pure imaginary. The eigenstate $\gamma_5\psi_n$ has an eigenvalue $-\lambda_n$, which in turn equals to λ_n^*. The Dirac determinant is, therefore, a product of all the paired eigenvalues $\lambda_n + m$ and $\lambda_n^* + m$, which is nonnegative because $|\lambda_n + m|^2 \geq 0$.

When μ_q is nonzero, $\gamma_4\mu_q$ is Hermitian and thus the eigenvalue λ_n defined by

$$(\gamma_\mu D^\mu + \gamma_4\mu_q)\psi_n = \lambda_n \psi_n \tag{3}$$

is no longer pure imaginary but complex. Here again, $\gamma_5\psi_n$ has an eigenvalue $-\lambda_n$, but it is different from λ_n^* in this case. Therefore, the Dirac determinant, given by $\prod_n(\lambda_n + m)(-\lambda_n + m)$ is not necessarily nonnegative, and when it is negative for some gauge configurations, the sign problem occurs.

Two-color QCD is unique in the sense that one can find another eigenstate $\sigma_2 C^{-1}\gamma_5\psi_n^*$ with an eigenvalue λ_n^*, where σ_2 is the second Pauli matrix in color space and C represents the charge conjugation. Obviously, the eigenstate multiplied by γ_5 has an eigenvalue $-\lambda_n^*$. Consequently, the eigenvalues of the Dirac operator always constitute a quartet: $\lambda_n + m$, $-\lambda_n + m$, $\lambda_n^* + m$, and $-\lambda_n^* + m$, leading to nonnegative Dirac determinant through the relation $|\lambda_n + m|^2| - \lambda_n + m|^2 \geq 0$. We note that our argument holds even with an odd number of quark flavors, although in this case the sign problem was supposed to occur [32].

We can thus conclude that *two-color QCD has no sign problem at finite density regardless of the number of quark flavors*. This implies that the Monte-Carlo simulation for two-color QCD with two flavors is feasible in the presence of both μ_q and μ_I, which would help us elucidate the phase structure.

C. Model for two-color quark matter

We turn to a model for two-color and two-flavor quark matter within the BCS ansatz that two particles with opposite momenta $\boldsymbol{p}$ and $-\boldsymbol{p}$ pair with a short-range interaction. We may then assume that only two mean fields, namely, the chiral and diquark condensates,

$$\sigma = G\langle\bar\psi_i^a\psi_i^a\rangle, \qquad \Delta = G\epsilon^{ij}\epsilon^{ab}\langle\psi_i^{Ta} iC\gamma_5\psi_j^b\rangle, \tag{4}$$

are predominant in the region $\mu_I < \mu_q$. We denote the color and flavor indices by a, b and i, j, respectively. Here, T represents the transposition in the Dirac index, and C is the charge conjugate matrix to make the diquark condensate Lorentz invariant. The dimensional coefficient G, which controls the strength of the four-fermi coupling constant, is common to the chiral and diquark condensates by virtue of the Pauli-Gürsey symmetry. In a rough but intuitively more understandable notation, $\sigma \sim \langle\bar u u\rangle + \langle\bar d d\rangle$ and $\Delta \sim \langle ud\rangle$. Note that when $\mu_I > \mu_q$, the predominant diquark condensate $\langle ud\rangle$ gives way to $\langle u\bar d\rangle$. In this work, however, we limit our discussion solely to the region $\mu_I < \mu_q$.

In the LOFF phase where a u-quark with the momentum $\boldsymbol{q} + \boldsymbol{p}$ and a d-quark with the momentum $\boldsymbol{q} - \boldsymbol{p}$ form a Cooper pair with the total momentum $2\boldsymbol{q}$, the diquark condensate has a spatially oscillating phase as

$$\Delta \to \Delta e^{i2\boldsymbol{q}\cdot\boldsymbol{r}}. \tag{5}$$

It should be noted that we neglect any spin-one condensate such as $\langle uu\rangle$, $\langle dd\rangle$, and $\langle\bar d\bar d\rangle$ entirely in this work. It generally coexists with the spin-zero condensate $\langle ud\rangle$ in the LOFF state but is known to be smaller by one order of magnitude than the spin-zero one [24]. We remark that the spin-one condensates could be relevant for even larger Fermi surface separation between u and d quarks [32].

Then, the thermodynamic potential with the mean-field condensates σ and Δ and the pair momentum $\boldsymbol{q}$ can be expressed as

$$\Omega(\sigma, \Delta, q; m_0, \mu_q, \mu_I) = -\frac{1}{4}\int^\Lambda \frac{d^3\boldsymbol{p}}{(2\pi)^3}\sum_{i=1}^{32}|\epsilon_i(\boldsymbol{p}, \boldsymbol{q})| + \frac{\sigma^2 + \Delta^2}{2G}. \tag{6}$$

Here Λ is the cutoff parameter and m_0 is the current quark mass. After the $\boldsymbol{p}$-integration, the thermodynamic potential no longer depends on the direction of the three-vector $\boldsymbol{q}$ but becomes a function of its magnitude $q = |\boldsymbol{q}|$ alone.

Expression (6) contains the sum of the quasiquark energies $\epsilon_i(\boldsymbol{p})$, which correspond to the 32 eigenvalues of the 32×32 quark Hamiltonian matrix with two colors, two flavors, two spins, quark-antiquark, and Nambu-Gor'kov doubling. The remaining part is the energy shift associated with the mean-field approximation. The condensates, σ and Δ, share the same coupling G as implied by the Pauli-Gürsey symmetry; in the chiral limit $m_0 = 0$ at $\mu_q = \mu_I = 0$, the thermodynamic potential Ω should be reduced to be a function of $\sigma^2 + \Delta^2$. This feature exemplifies a great advantage of two-color QCD over various model studies of real QCD in which quantities affected by chiral dynamics strongly depend on the model parameters.

When $\Delta = \mu_I = 0$, all quarks have the same constituent mass, $M = m_0 - \sigma$, leading to the quark and antiquark energies, $\xi(\boldsymbol{p}) \mp \mu_q$ with $\xi(\boldsymbol{p}) = \sqrt{\boldsymbol{p}^2 + M^2}$. The effect of nonzero μ_I is to shift μ_q by $+\mu_I$ and $-\mu_I$ for u and d quarks, that is,

$$\mu_u = \mu_q + \mu_I, \qquad \mu_d = \mu_q - \mu_I, \tag{7}$$

which results in crossing of the energy levels. In the presence of the diquark condensate Δ, the crossing energy levels mix together and a level repulsion occurs. We will simply approximate the energy levels by mixing between the u-quark energy $\xi(\boldsymbol{q}+\boldsymbol{p})-\mu_u$ and the d-quark energy $\xi(\boldsymbol{q}-\boldsymbol{p})-\mu_d$. Of course we can also swap $\boldsymbol{q}+\boldsymbol{p}$ and $\boldsymbol{q}-\boldsymbol{p}$ but the integration over $\boldsymbol{p}$ washes out the difference eventually. The eigenvalues of the following 2×2 matrix,

$$\begin{bmatrix} \xi(\boldsymbol{q}+\boldsymbol{p})-\mu_u & \Delta \\ \Delta & -\xi(\boldsymbol{q}-\boldsymbol{p})+\mu_d \end{bmatrix}, \tag{8}$$

give the quasiquark energy dispersion relations,

$$\epsilon_{\mathrm{p}}^{\pm}(\boldsymbol{p},\boldsymbol{q}) = \left| \frac{1}{2}\delta\xi(\boldsymbol{p},\boldsymbol{q}) \pm \mu_{\mathrm{I}} + \sqrt{[\bar{\xi}(\boldsymbol{p},\boldsymbol{q})-\mu_{\mathrm{q}}]^2+\Delta^2} \right|, \tag{9}$$

with

$$\delta\xi(\boldsymbol{p},\boldsymbol{q}) = \xi(\boldsymbol{q}+\boldsymbol{p})-\xi(\boldsymbol{q}-\boldsymbol{p}), \tag{10}$$

$$\bar{\xi}(\boldsymbol{p},\boldsymbol{q}) = \tfrac{1}{2}[\xi(\boldsymbol{q}+\boldsymbol{p})+\xi(\boldsymbol{q}-\boldsymbol{p})]. \tag{11}$$

Note that there are eightfold degeneracies for $\epsilon_{\mathrm{p}}^{+}(\boldsymbol{p})$ and $\epsilon_{\mathrm{p}}^{-}(\boldsymbol{p})$, respectively, which implies 16 energy levels in total. We should remark that these energy dispersion relations are slightly different from those used in Ref. [24] because the gap energy Δ is constant in our approximation instead of depending on the relative angle of $\boldsymbol{q}+\boldsymbol{p}$ and $\boldsymbol{q}-\boldsymbol{p}$. It is straightforward to introduce any $\boldsymbol{q}$ dependence in Δ. We will, however, stick to a constant Δ, partly because we will confirm later that a constant Δ is enough to reproduce results quantitatively consistent with Ref. [24] and partly because no reliable ansatz is in hand *a priori* except when M is zero.

As for the antiquark contribution, dropping Δ is a good approximation as long as $\Delta \ll M+\mu_{\mathrm{q}}$. Such an approximation, however, would apparently ruin the Pauli-Gürsey symmetry which should be present in the limit of $m_0=\mu_{\mathrm{q}}=\mu_{\mathrm{I}}=\boldsymbol{q}=0$. Hence, we shall keep Δ as well as σ also for the antiquark energy levels by adopting the same form of the energy dispersion relations as the quark contribution with $-\mu_{\mathrm{q}}$ replaced by $+\mu_{\mathrm{q}}$:

$$\epsilon_{\mathrm{a}}^{\pm}(\boldsymbol{p},\boldsymbol{q}) = \left| \frac{1}{2}\delta\xi(\boldsymbol{p},\boldsymbol{q}) \pm \mu_{\mathrm{I}} + \sqrt{[\bar{\xi}(\boldsymbol{p},\boldsymbol{q})+\mu_{\mathrm{q}}]^2+\Delta^2} \right| \tag{12}$$

with eightfold degeneracies again, although the difference of $\epsilon_{\mathrm{a}}^{\pm}(\boldsymbol{p},\boldsymbol{q})$ from $|\xi(\boldsymbol{q}+\boldsymbol{p})+\mu_u|$ and $|\xi(\boldsymbol{q}-\boldsymbol{p})+\mu_d|$ is merely negligible. We do not consider the mixing between quarks and antiquarks which would take place with nonvanishing $\langle u\bar{d}\rangle$ when $\mu_{\mathrm{I}}>\mu_{\mathrm{q}}$.

Using the thermodynamic potential as specified above, we will solve the following equations:

$$\frac{\partial\Omega}{\partial\sigma}=0, \qquad \frac{\partial\Omega}{\partial\Delta}=0, \qquad \frac{\partial\Omega}{\partial q}=0, \tag{13}$$

to obtain the self-consistent values of Δ, σ, and q. Now that we have come by all the necessary formulas, we will proceed to numerics next.

III. RESULTS

In this section we will present the numerical solutions to Eq. (13) obtained for the isotropic superfluid phase, the gapless phase, and the LOFF phase. The gapless phase is unstable, but still we will investigate the gapless solution to Eq. (13) for the later purpose of surveying the energy landscape.

For numerical evaluations we first have to fix the model parameters, namely, the current quark mass m_0, the cutoff Λ, and the four-fermi coupling constant G. We do not need to specify Λ because we will present all the dimensional quantities in units of Λ. Instead of G we will use the diquark condensate at $\mu_{\mathrm{I}}=0$ denoted by $\Delta_0(\mu_{\mathrm{q}})$ to specify the interaction strength; a larger Δ_0 means a stronger coupling. In this paper we will take two parameter choices:

$$\text{Parameter I:} \quad m_0=0, \quad \Delta_0(\mu_{\mathrm{q}}=0.5\Lambda)=0.05\Lambda, \tag{14}$$

and

$$\text{Parameter II:} \quad m_0=0.025\Lambda, \quad \Delta_0(\mu_{\mathrm{q}}=0.5\Lambda)=0.5\Lambda. \tag{15}$$

Hereafter we will refer to Parameter I as the *weak coupling* parameter set since it will allow us to confirm that our approach recovers the known properties of the LOFF phase at weak coupling. For Parameter II, which will be denoted by the *intermediate coupling* parameter set, the choice of m_0 is motivated by available lattice simulations of two-color QCD. As we can see in Fig. 1, for Parameter II, the chiral and diquark condensates amount to a comparable magnitude. In the absence of the sign problem of the Dirac determinant even with μ_{I} introduced as discussed in Sec. II B, our results at intermediate coupling could be readily compared with what we would observe from lattice simulations.

A. (Fully gapped) superfluid phase

We show in Fig. 1 the behavior of the chiral and diquark condensates as a function of the quark chemical potential μ_{q} at $\mu_{\mathrm{I}}=\boldsymbol{q}=0$. The condensates at weak coupling with Parameter I (14) are exponentially suppressed for small μ_{q}. This suppression is a sharp contrast to the results in the strong coupling limit [42,43]. In particular σ keeps vanishing entirely because of $m_0=0$ as first noted in Ref. [42]. From Fig. 1 we can make sure that $\Delta_{\mathrm{I}}(\mu_{\mathrm{q}}=0.5\Lambda)=0.05\Lambda$ is satisfied. In the case of intermediate coupling with Parameter II (15), on the other hand, the diquark

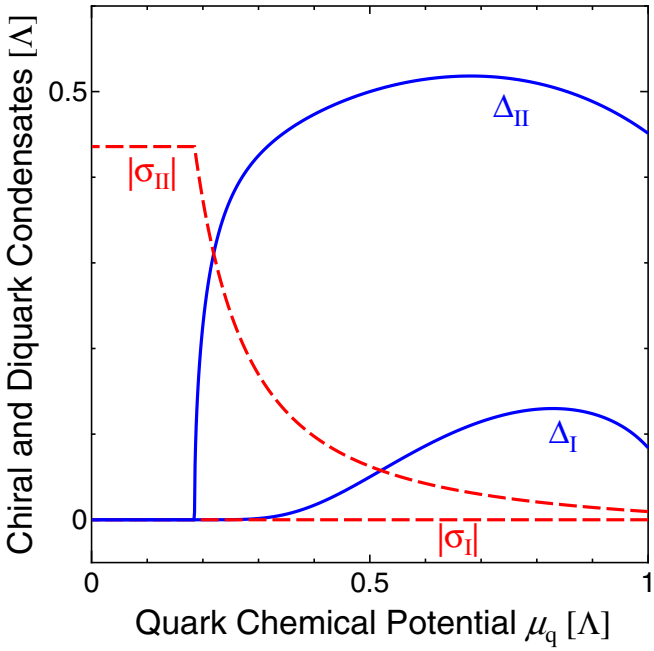

FIG. 1 (color online). Chiral and diquark condensates as a function of μ_q at $\mu_I = q = 0$, given in unit of Λ. The quantities with the subscript "I" and "II" are the results obtained at weak and intermediate coupling, respectively.

condensate appears above the threshold $\mu_q = 0.185\Lambda$. We can confirm that $\Delta_{II}(\mu_q = 0.5\Lambda) = 0.5\Lambda$ as it should. The nonmonotonic behavior of Δ at $\mu_q \gtrsim 0.7$ is caused by the *saturation* effect: The density cannot grow unboundedly because the phase space is limited by the presence of Λ, which is observed in lattice simulations as well as in model studies [33,43]. We remark that our Δ_{II} and $|\sigma_{II}|$ are to be compared with the results given in Figs. 1 and 2 of Ref. [33].

B. Gapless phase

The isospin chemical potential μ_I plays a role in exerting stress onto quarks to tear the Cooper pair apart. As long as $\mu_I < \Delta$, the isotropic (fully gapped) superfluid phase is rigid against such stress. This can be easily understood from Eq. (9) with $q = 0$ substituted; if $\mu_I < \Delta$ and $q = 0$, then $\epsilon_p^+ + \epsilon_p^- = 2\sqrt{(\xi - \mu_q)^2 + \Delta^2}$, which has no dependence on μ_I, and thus Δ and σ stay constant regardless of μ_I.

Once μ_I becomes larger than Δ, ϵ_p^- decreases down to zero at $p \sim \mu_q$, that is, the energy dispersion relation become breached or gapless. This breached or gapless superfluid solution is similar to the gapless 2SC (g2SC) phase known from QCD. It is because the gap equation in the two-color problem takes the same form as in the 2SC phase. In contrast to the g2SC case, we do not impose neutrality on the present system. In principle, we can consider electric neutrality by turning the electromagnetic interaction on and putting electrons into the system. We will not do so, however, partly because the resultant stability of the gapless state with respect to homogeneous change in the gap amplitude as seen in the g2SC case would not be of interest here, and partly because we intend to keep an interesting resemblance of the present system with electric charge turned off and μ_I introduced to atomic Fermi gases with population imbalance created in low temperature experiments. Note that even for charged systems, the gapless superfluid state is generally unstable with respect to inhomogeneous fluctuations in the order parameter [17].

The typical behavior of the diquark condensate as a function of μ_I is plotted in Fig. 2 for the weak and intermediate coupling cases. Both are the results at $\mu_q = 0.5\Lambda$ and thus the superfluid solution stays at $\Delta = 0.05\Lambda$ for Parameter I and at $\Delta = 0.5\Lambda$ for Parameter II in the figure. There appear two branches in the solutions to Eq. (13) for a finite range of μ_I, namely, the gapless solution and the superfluid solution. When these two solutions meet at a certain μ_I, the gap equations cease to have any solution. It happens at $\mu_I = 0.099\Lambda$ for Parameter I and $\mu_I = 0.99\Lambda$ for Parameter II in Fig. 2. As we shall see from the energy landscape, the thermodynamic potential Ω has an inflection point when one solution corresponding to a local minimum of the potential meets the other corresponding to a local maximum. This means that there must exist another state which takes over the ground state before μ_I reaches the meeting point. In fact, a first-order phase transition to normal matter is found at $\mu_I = 0.0355\Lambda$ or, equivalently,

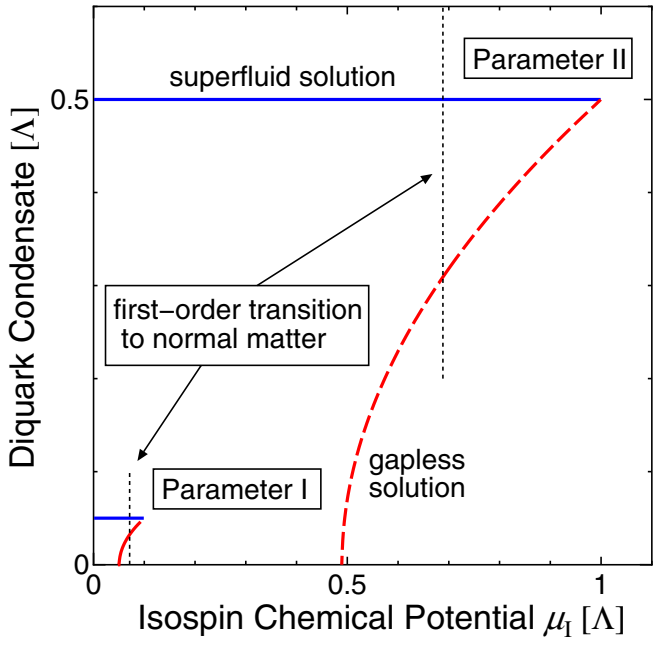

FIG. 2 (color online). Superfluid and gapless solutions at $\mu_q = 0.5\Lambda$. The first-order phase transition from superfluid to normal quark matter is indicated by the dotted line.

$$\mu_I = 0.711\Delta_0 \qquad \text{(for Parameter I)}, \tag{16}$$

where $\Delta_0 = 0.05\Lambda$ at weak coupling, and $\mu_I = 0.344\Lambda$ or, equivalently,

$$\mu_I = 0.688\Delta_0 \qquad \text{(for parameter II)}, \tag{17}$$

where $\Delta_0 = 0.5\Lambda$ at intermediate coupling. As discussed in Ref. [24], this μ_I of the first-order transition approximately gives the lower bound $\delta\mu_2$ of the LOFF favored region if the upper bound $\delta\mu_1$ of the LOFF solution, as will be discussed later, is greater than $\delta\mu_2$. The point is that the energy gain in the LOFF phase relative to normal quark matter is tiny as compared with the scale of the change in the energy difference between the superfluid and normal phases with increasing μ_I. In order for the LOFF phase to be most favorable, therefore, it is necessary that the energy gain in the superfluid phase be very close to zero, which is only possible when μ_I is very close to the first-order phase transition point. We note that our weak coupling value of $\delta\mu_2 = 0.711\Delta_0$ precisely agrees with the known result in Ref. [24].

C. LOFF phase

Let us now move on to the central part of this paper that addresses the LOFF favored region in μ_q–μ_I space. Here we shall discuss the weak and intermediate coupling cases separately.

In the presence of nonzero $\boldsymbol{q}$, the free energy has an unphysical term proportional to $-\Lambda^2 q^2$ which must be subtracted. It is a nontrivial problem how to renormalize this spurious contribution properly in a field-theoretical procedure. [See discussions in Refs. [9,10] about this problem in evaluating the Meissner mass.] Our preference is to follow a practical prescription here. After we solve the gap equations with a given $\boldsymbol{q}$ to get $\sigma = \sigma(\Delta, q)$, which is not affected by the term $\sim -\Lambda^2 q^2$ in question, we can define the subtracted free energy as

$$\Omega_s(\Delta, q) = \Omega[\sigma(\Delta, q), \Delta(q), q] - \Omega[\sigma(\Delta, q), 0, q], \tag{18}$$

in order to determine the gap Δ and the optimal value of q from its global minimum. This prescription is the simplest choice consistent with the fact that Ω_s should be flat in the q-direction in the absence of finite Δ. The second term in the right-hand side could be $-\Omega[\sigma(0, q), 0, q]$, but it would make only a negligible difference in numerical outputs.

1. Weak coupling case

We can solve the gap equation $\partial\Omega_s/\partial\Delta = 0$ to obtain $\Delta = \Delta(q)$ as a function of q. Figure 3 shows the numerical results for $\Delta(q)$ with Parameter I (weak coupling) for several values of μ_I in the vicinity of the critical value $\mu_I = \delta\mu_2$. We can observe from the curve labeled with $\mu_I = 0.033\Lambda$ that $\Delta(q)$ is smoothly connected up to the value at $q = 0$ which corresponds to the diquark condensate in the superfluid phase. It is clear from Ω_s plotted in Fig. 4 that, when $\mu_I = 0.033\Lambda$, the superfluid phase at $q = 0$ has a much smaller energy than the metastable LOFF solution at $q \neq 0$. Interestingly the LOFF solution becomes disconnected from the superfluid solution as μ_I grows up. Nevertheless, the superfluid phase continues to

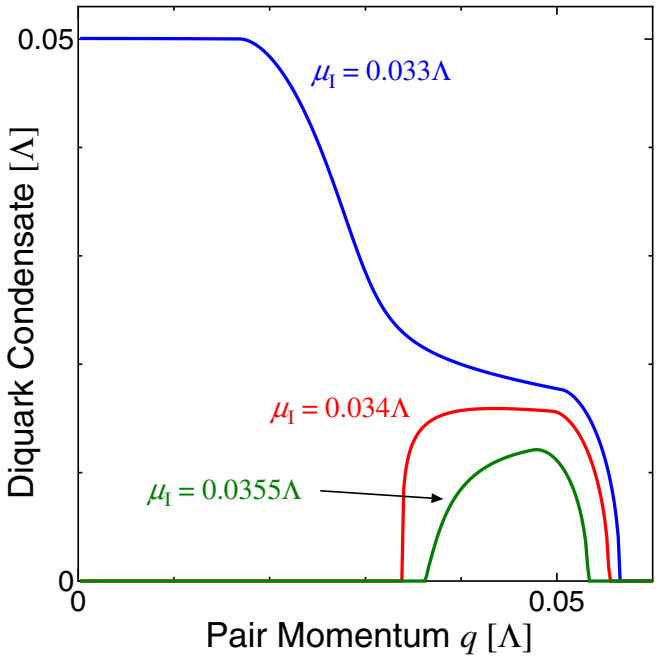

FIG. 3 (color online). Diquark condensate at weak coupling as a function of the pair momentum q, which is calculated for $\mu_I = 0.033\Lambda$ (top), 0.034Λ (middle), and 0.0355Λ (bottom).

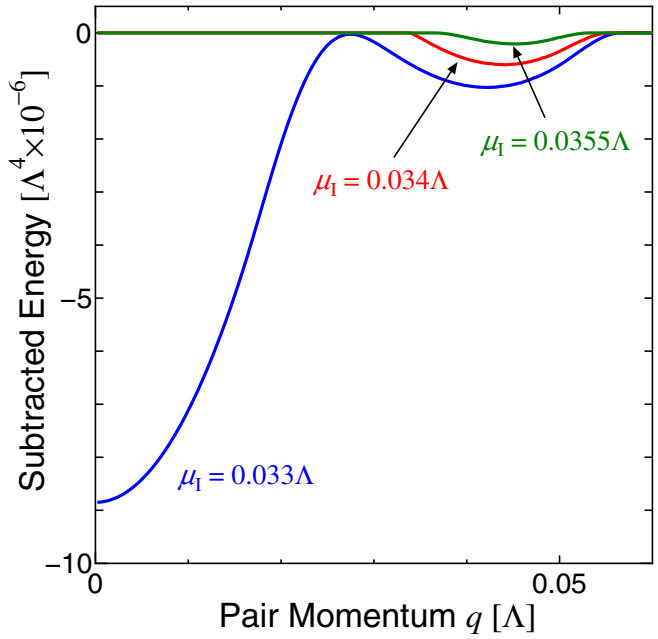

FIG. 4 (color online). Energy difference (18) at weak coupling as a function of the pair momentum q. The three curves correspond to those displayed in Fig. 3.

exist separately and is more favorable until the LOFF phase turns to the ground state at $\mu_I > \delta\mu_2$.

Then, there occurs a crucial question: How large is the upper bound $\delta\mu_1$ of μ_I at which the LOFF solution disappears? The q-range of nonzero $\Delta(q)$ shrinks as μ_I gets larger as indicated in Fig. 3. We find that it is located at $\mu_I = 0.0377\Lambda$ or, equivalently,

$$\delta\mu_1 = 0.755\Delta_0, \tag{19}$$

where $\Delta_0 = 0.05\Lambda$, and that the optimal pair momentum at $\mu_I = \delta\mu_1$ reads $q = 0.045\Lambda$ or, equivalently,

$$q \simeq 1.2\delta\mu_1. \tag{20}$$

Our $\delta\mu_1$ and optimal q are very close to the values reported in Ref. [24] in the weak coupling limit: $\delta\mu_1 = 0.754\Delta_0$ and $q = 1.20\Delta_0$. We are thus confident that our method is thoroughly consistent with the existing analyses.

It would be intriguing to turn our focus toward an even higher density region where the saturation effect is relevant. Then, the above result for the LOFF favored region, $\delta\mu_1 = 0.755\Delta_0 > \mu_I > \delta\mu_2 = 0.711\Delta_0$, may well be altered, and indeed the LOFF window enlarges a bit.

Figure 5 demonstrates that the LOFF window varies with changing quark chemical potential μ_q. The shape of the curves reflects that of $\Delta_0(\mu_q)$ given in Fig. 1. The LOFF window becomes slightly wider in the region where the saturation effect is sufficient to make the curves have a negative slope. For instance, at $\mu_q = 0.95\Lambda$ the LOFF favored region is bounded by

$$\begin{aligned} \delta\mu_1 &= 0.080\Lambda = 0.73\Delta_0(\mu_q = 0.95\Lambda), \\ \delta\mu_2 &= 0.069\Lambda = 0.62\Delta_0(\mu_q = 0.95\Lambda), \end{aligned} \tag{21}$$

where $\Delta_0 = 0.110\Lambda$. The interval between them is not substantial in the weak coupling case, while the behavior drastically changes at intermediate coupling as we will see shortly.

2. Intermediate coupling case

In the intermediate coupling case with Parameter II, the gross behavior of the diquark condensate and the subtracted energy as a function of q is just similar to what we have shown in Figs. 3 and 4. We thus find that such behavior has only a weak dependence on the parameter choice. For the LOFF favored region, however, the parameter dependence is important as can be seen from comparison between Figs. 5 and 6.

The first-order transition from the superfluid to the normal phase occurs above the upper bound of the LOFF solution for $\mu_q \lesssim 0.7\Lambda$. This means that the LOFF window shuts there and the superfluid phase remains the ground state even for $\mu_I > \delta\mu_1$ until normal quark matter appears. This behavior, which is a contrast to the case with Parameter I, is caused by stronger coupling rather than by heavier m_0. In fact, the chiral condensate is so small compared with the diquark condensate at $\mu_q \sim 0.7\Lambda$ as shown in Fig. 1 that it hardly affects the phase boundaries.

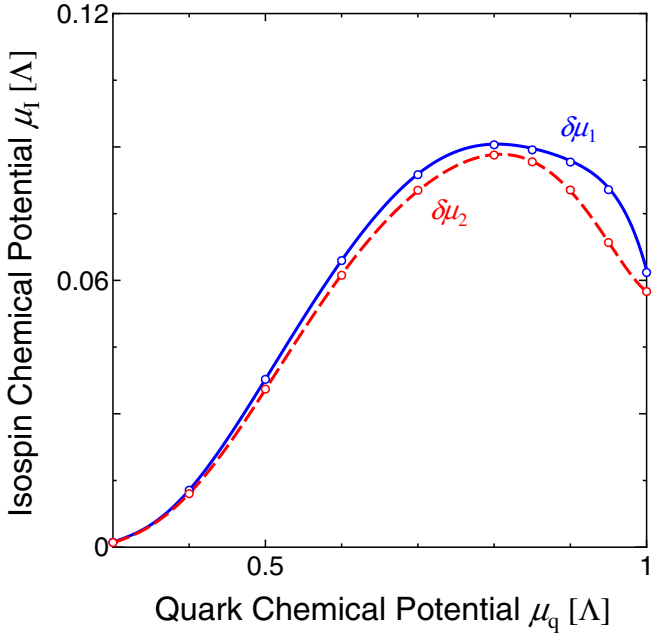

FIG. 5 (color online). The LOFF favored region bounded by $\delta\mu_1$ and $\delta\mu_2$, calculated at weak coupling as a function of μ_q. The open circles represent the calculated values, whereas the curves are interpolations between the neighboring circles by splines.

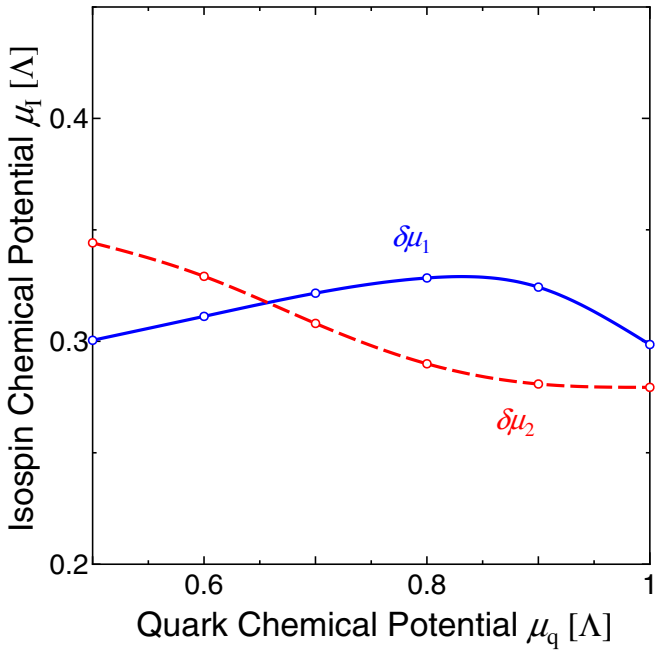

FIG. 6 (color online). Same as Fig. 5 except that calculations are performed at intermediate coupling. Note that the LOFF region corresponds to the region of large μ_q in which $\delta\mu_1$ is larger than $\delta\mu_2$.

The LOFF window opens at $\mu_q \gtrsim 0.7\Lambda$ where we find the same tendency as the weak coupling case that the LOFF window widens by the saturation effect. At $\mu_q = 0.8\Lambda$, for instance, the bounds of the LOFF window are given by

$$\delta\mu_1 = 0.33\Lambda = 0.64\Delta_0(\mu_q = 0.8\Lambda),$$
$$\delta\mu_2 = 0.29\Lambda = 0.57\Delta_0(\mu_q = 0.8\Lambda), \quad (22)$$

where $\Delta_0 = 0.51\Lambda$ at $\mu_q = 0.8\Lambda$.

We note that our plane-wave LOFF ansatz (5) is only the simplest one. If we consider a more general three-dimensional crystalline structure, the LOFF favored region has to be even wider. We would stress that our results shown in Fig. 6 strongly support the possibility of probing the generic crystalline color superconducting phase, along with the isotropic superfluid phase, with numerical approach on lattice. In fact, the values of μ_I at which the LOFF phase occurs are less than a half of μ_q, while being larger than the inverse of a typical lattice size. Possible simulation to detect the LOFF phase would not require weaker coupling, finer lattice, or larger lattice.

We conclude this subsection by noting that the spin-one condensates would remain nonvanishing even above $\delta\mu_1$ because they can be formed between quarks of the same flavor irrespective of the Fermi surface mismatch [32].

D. Energy landscape

We will take a further look at the LOFF phase found at intermediate coupling. Let us pick up a point of $\mu_q = 0.8\Lambda$ and $\mu_I = 0.3\Lambda$ inside the LOFF favored region illustrated in Fig. 6. In order to elucidate how the unstable gapless phase is connected to the LOFF phase, we picture the energy landscape, namely, we plot Ω_s as a function of Δ and q as shown in Fig. 7.

It is obvious from Fig. 7 that the LOFF phase sits certainly at the global minimum of the potential energy landscape. The local minimum at $\Delta = q = 0$ is normal quark matter, another local minimum at $\Delta \neq 0$ and $q = 0$ is the metastable superfluid phase, and the in-between local maximum along the Δ-axis corresponds to the unstable gapless phase. The gapless phase is unstable with respect to fluctuations in any direction in the space of $\boldsymbol{q}$ and Δ. Specifically, the instability along the Δ direction is the Sarma instability originally noticed in Ref. [4]. In the g2SC or gCFL phase, the remedy against the Sarma instability comes from the electric and color neutrality conditions. Even with neutrality imposed, however, the instability in the q direction is still a problem, which is nothing but the chromomagnetic instability in the g2SC or gCFL phase. For a neutral superfluid of interest here, it is the phase instability.

Figure 8 is the contour density plot of the numerical data in Fig. 7, which allows us to describe graphically what we mentioned above. The gapless phase has instabilities leading to normal quark matter, the isotropic superfluid phase,

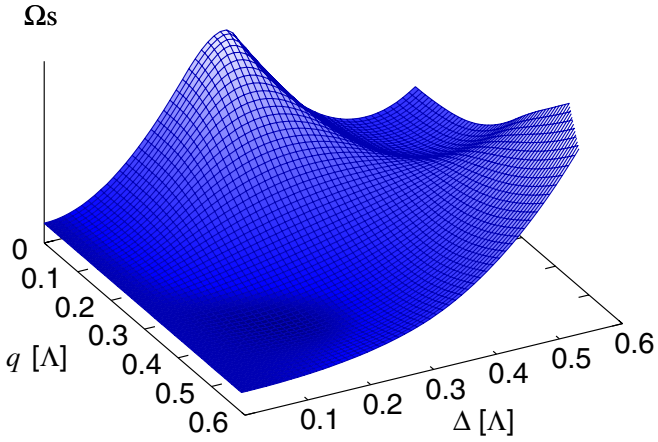

FIG. 7 (color online). Subtracted free energy as a function of Δ and q with $M = M(\Delta, q)$ which is the solution to the gap equation. A darker colored region has a smaller energy. The LOFF phase is the global minimum of the energy.

and the LOFF phase, among which the LOFF phase has the lowest energy. This contour plot presumably captures the essence of the instability problem and its implications for QCD quark matter. We would anticipate that the energy landscape around the g2SC phase is more or less similar to Fig. 8 except that the gapless phase is stabilized against fluctuations in Δ, that is, the gapless state is a saddle point on the energy landscape. It is hard, however, to imagine what would happen in the case of the gCFL phase with three flavors, because there are three predominant diquark condensates. In large dimensional space spanned by more variational parameters, it is not straightforward to see whether the instability in the gapless phase is directly connected to the LOFF phase. There could be several distinct LOFF solutions as conjectured in Ref. [16]. It would be a challenging problem to draw the energy landscape in the three-flavor case and to confirm that the

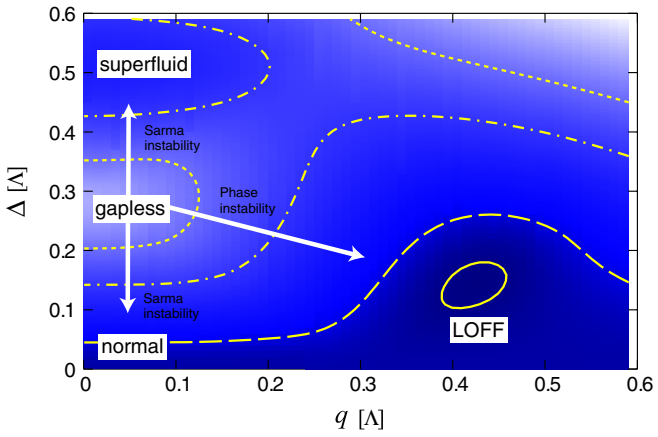

FIG. 8 (color online). Contour density plot of Ω_s, which indicate two minima corresponding to the metastable superfluid phase and the ground state of the LOFF phase and one maximum corresponding to the unstable gapless phase.

instability is responsible for the LOFF phase, as we have done successfully in two-color and two-flavor QCD in this work.

IV. CONCLUSIONS

We investigated the LOFF favored window of μ_{I} for two-color and two-flavor QCD using a mean-field model. First, we satisfactorily reproduced the known results at weak coupling. We then performed our calculation for a set of the model parameters in which the coupling strength is intermediate and thus relevant to currently available lattice simulations. We found out a nonzero interval of μ_{I} where the single plane-wave LOFF phase is energetically more favorable than the isotropic superfluid phase and normal quark matter. For intermediate coupling, we took a close look at the energy landscape to see the relation of the Sarma and phase instabilities associated with the gapless solution of the gap equations with the LOFF phase.

In this work we do not take account of any possibility of the mixed phase or the phase separation for a nonzero range of μ_{q} as discussed in Ref. [17] because we turn electric charge off in the present system. The chargeless limit would be advantageous to lattice two-color QCD simulation. In the absence of the fermion sign problem, furthermore, we believe that the lattice approach to the LOFF phase is feasible [44].

ACKNOWLEDGMENTS

We thank Atsushi Nakamura and Chiho Nonaka for discussions. K. F. thanks Masakiyo Kitawaza for comments. He also thanks Sinya Aoki, Yasumichi Aoki, and Shinji Ejiri for conversations. This research was supported in part by RIKEN BNL Research Center and the U.S. Department of Energy under cooperative research agreement No. DE-AC02-98CH10886.

[1] For a review, see, K. Rajagopal and F. Wilczek, arXiv:hep-ph/0011333.
[2] M. G. Alford, K. Rajagopal, and F. Wilczek, Nucl. Phys. **B537**, 443 (1999).
[3] M. Huang and I. Shovkovy, Phys. Lett. B **564**, 205 (2003); Nucl. Phys. **A729**, 835 (2003).
[4] G. Sarma, J. Phys. Chem. Solids **24**, 1029 (1963).
[5] E. Gubankova, W. V. Liu, and F. Wilczek, Phys. Rev. Lett. **91**, 032001 (2003).
[6] M. Alford, C. Kouvaris, and K. Rajagopal, Phys. Rev. Lett. **92**, 222001 (2004); Phys. Rev. D **71**, 054009 (2005).
[7] M. Huang and I. A. Shovkovy, Phys. Rev. D **70**, 051501 (2004); **70**, 094030 (2004).
[8] R. Casalbuoni, R. Gatto, M. Mannarelli, G. Nardulli, and M. Ruggieri, Phys. Lett. B **605**, 362 (2005); **615**, 297(E) (2005).
[9] M. Alford and Q. h. Wang, J. Phys. G **31**, 719 (2005).
[10] K. Fukushima, Phys. Rev. D **72**, 074002 (2005); see also,arXiv:hep-ph/0510299.
[11] S. B. Ruster, I. A. Shovkovy, and D. H. Rischke, Nucl. Phys. **A743**, 127 (2004).
[12] K. Iida, T. Matsuura, M. Tachibana, and T. Hatsuda, Phys. Rev. Lett. **93**, 132001 (2004); Phys. Rev. D **71**, 054003 (2005).
[13] K. Fukushima, C. Kouvaris, and K. Rajagopal, Phys. Rev. D **71**, 034002 (2005).
[14] H. Abuki and T. Kunihiro, Nucl. Phys. **A768**, 118 (2006).
[15] I. Giannakis and H. C. Ren, Phys. Lett. B **611**, 137 (2005).
[16] K. Fukushima, Phys. Rev. D **73**, 094016 (2006).
[17] K. Iida and K. Fukushima, Phys. Rev. D **74**, 074020 (2006).
[18] I. Giannakis, D. Hou, M. Huang, and H. c. Ren, Phys. Rev. D **75**, 011501 (2007).
[19] A. I. Larkin and Yu. N. Ovchinnikov, Sov. Phys. JETP **20**, 762 (1965).
[20] P. Fulde and R. A. Ferrell, Phys. Rev. **135**, A550 (1964).
[21] M. Huang, Phys. Rev. D **73**, 045007 (2006).
[22] T. Schäfer, Phys. Rev. Lett. **96**, 012305 (2006).
[23] E. V. Gorbar, M. Hashimoto, and V. A. Miransky, Phys. Lett. B **632**, 305 (2006).
[24] M. G. Alford, J. A. Bowers, and K. Rajagopal, Phys. Rev. D **63**, 074016 (2001).
[25] J. A. Bowers, J. Kundu, K. Rajagopal, and E. Shuster, Phys. Rev. D **64**, 014024 (2001).
[26] J. Kundu and K. Rajagopal, Phys. Rev. D **65**, 094022 (2002).
[27] R. Casalbuoni and G. Nardulli, Rev. Mod. Phys. **76**, 263 (2004).
[28] J. A. Bowers and K. Rajagopal, Phys. Rev. D **66**, 065002 (2002).
[29] R. Casalbuoni, R. Gatto, N. Ippolito, G. Nardulli, and M. Ruggieri, Phys. Lett. B **627**, 89 (2005); **634**, 565(E) (2006).
[30] K. Rajagopal and R. Sharma, Phys. Rev. D **74**, 094019 (2006).
[31] M. Mannarelli, K. Rajagopal, and R. Sharma, arXiv:hep-ph/0702021 [Phys. Rev. D (to be published)].
[32] K. Splittorff, D. T. Son, and M. A. Stephanov, Phys. Rev. D **64**, 016003 (2001).
[33] C. Ratti and W. Weise, Phys. Rev. D **70**, 054013 (2004).
[34] J. B. Kogut, D. Toublan, and D. K. Sinclair, Phys. Lett. B **514**, 77 (2001).
[35] J. B. Kogut, D. K. Sinclair, S. J. Hands, and S. E. Morrison, Phys. Rev. D **64**, 094505 (2001).
[36] J. B. Kogut, D. Toublan, and D. K. Sinclair, Nucl. Phys. **B642**, 181 (2002).

[37] S. Muroya, A. Nakamura, and C. Nonaka, Phys. Lett. B **551**, 305 (2003).
[38] S. Muroya, A. Nakamura, C. Nonaka, and T. Takaishi, Prog. Theor. Phys. **110**, 615 (2003).
[39] S. Hands, S. Kim, and J. I. Skullerud, Eur. Phys. J. C **48**, 193 (2006).
[40] A. Smilga and J. J. M. Verbaarschot, Phys. Rev. D **51**, 829 (1995).
[41] K. Fukushima and Y. Hidaka, Phys. Rev. D **75**, 036002 (2007) and references therein.
[42] E. Dagotto, F. Karsch, and A. Moreo, Phys. Lett. **169B**, 421 (1986).
[43] Y. Nishida, K. Fukushima, and T. Hatsuda, Phys. Rep. **398**, 281 (2004).
[44] K. Fukushima, K. Iida, A. Nakamura, and C. Nonaka (work in progress).